Wavelet analysis in multiplicity fluctuations

Ding-wei Huang
Department of Physics, Chung Yuan Christian University, Chung-li, Taiwan
(Received 15 January 1997)

A wavelet analysis is applied to the study of correlations in multiplicity fluctuations. Both the usual correlation functions as well as the wavelet transformed functions are calculated and compared with three different models: the FRITIOF, random cascade, and Ising models. The large off-diagonal bin correlations are effectively suppressed by the wavelets. The correlations from different scales nearly decouple. The wavelet analysis provides a useful tool for studying the self-similarity of multiparticle production in high-energy collisions. [S0556-2821(97)03217-7]

PACS number(s): 11.80.La, 13.85.Hd

I. INTRODUCTION

Self-similar fluctuations are observed in many different stochastic processes, such as turbulence and phase transitions. Generally, a powerlike behavior of the correlation function is expected. Analyses of such fluctuations by means of wavelets have gained widespread applications, most notably in signal processing and data compression [1–4]. Recently, wavelets have also been proposed to study the possible fractal structure in multiparticle production processes [5]. A similar analysis has been applied to analyze the pseudorapidity distributions of high multiplicity JACEE events [6]. The formation of a disoriented chiral condensate in high-energy collisions, which is related to the chiral phase transition, can also be studied by wavelets [7]. And most recently, the wavelets have also been used for pattern recognition in high multiplicity events of heavy ion collisions [8].

The central property of wavelet analysis is the expansion with respect to a self-similar set of orthogonal basis functions, so-called wavelets. The entire basis is constructed from dilations and translations of one single function. It provides a convenient representation for studying the self-similar processes, in which an arbitrary distribution can be resolved simultaneously in many scales. Wavelet analysis has been successfully applied in studying the random cascade p model [5]. Along the same line, in this study wavelet analysis is applied to a more realistic model of multiparticle production: the FRITIOF model [9], which has been widely adopted as Monte Carlo simulations to experimental results. The observed fluctuations are also compared with two idealized models: the random cascade model [10] and the Ising model [11]. In the former the self-similar pattern is built-in; in the latter only the nearest-neighbor interactions are presented. The random cascade model has been used as a simple discrete approximation to multiparticle processes in high energy e^+e^- and hadron-hadron collisions, the so-called α model [12,13]. With the lattice-gas interpretation the Ising model has also been used recently to describe multiproduction processes [14].

In Sec. II the concept of wavelet analysis is briefly reviewed. In Sec. III the conventional bin correlations and the wavelet correlations are calculated in three different models: the FRITIOF, random cascade, and Ising models. Discussions and conclusions are presented in Sec. IV.

II. MULTIRESOLUTION ANALYSIS

In this section the basic ingredients of wavelet analysis are briefly summarized for application in multiparticle fluctuations. A more detailed introduction to wavelets can be found elsewhere [1–4].

Consider an arbitrary distribution $n(x)$ within the interval $x\in[0,1]$. With the resolution of 2^J bins, the distribution $n(x)$ can be approximated by a histogram $n^{(J)}(x)$ as

$$n(x)\sim n^{(J)}(x)=\sum_{k=0}^{2^J-1} n_{Jk}\Phi_{Jk}(x), \tag{1}$$

where $\Phi_{Jk}(x)$ are simple box functions defined as

$$\Phi_{Jk}(x)=\begin{cases} 1 & \text{for } \dfrac{k}{2^J}\leqslant x<\dfrac{k+1}{2^J} \\ 0 & \text{otherwise.}\end{cases} \tag{2}$$

Notice that the 2^J box functions $\Phi_{Jk}(x)$ are orthogonal to one another. In this respect the coefficients n_{Jk} can be interpreted as amplitudes of the orthogonal expansion of $n^{(J)}(x)$ in terms of the basis functions $\Phi_{Jk}(x)$.

At the rougher resolution scale $(J-1)$, i.e., with 2^{J-1} bins, one has the following expansion,

$$n^{(J)}(x)\sim \sum_{k=0}^{2^{(J-1)}-1} n_{J-1,k}\Phi_{J-1,k}(x). \tag{3}$$

Notice that the 2^{J-1} box functions $\Phi_{J-1,k}(x)$ are again orthogonal to one another, but not orthogonal to the box functions $\Phi_{Jk}(x)$ at scale J. As the resolution is rougher, obviously some detail is lost compared to the expansion at scale J, Eq. (1). The lost detail is the difference between the expansions at scales J and $J-1$, which can be represented by the difference functions $\Psi_{J-1,k}(x)$ defined as

$$\Psi_{J-1,k}(x)=2\ \ \Phi_{J,2k}(x)-\Phi_{J-1,k}(x)$$

$$=\begin{cases} 1 & \text{for } \dfrac{k}{2^{J-1}}\leqslant x<\dfrac{k+0.5}{2^{J-1}} \\ -1 & \text{for } \dfrac{k+0.5}{2^{J-1}}\leqslant x<\dfrac{k+1}{2^{J-1}} \\ 0 & \text{otherwise,} \end{cases} \tag{4}$$

or, equivalently,

$$\Phi_{J,2k}(x)=\tfrac{1}{2}[\Phi_{J-1,k}(x)+\Psi_{J-1,k}(x)], \tag{5}$$

$$\Phi_{J,2k+1}(x)=\tfrac{1}{2}[\Phi_{J-1,k}(x)-\Psi_{J-1,k}(x)]. \tag{6}$$

Again, the 2^{J-1} difference functions $\Psi_{J-1,k}(x)$ are orthogonal to one another; they are also orthogonal to the box functions $\Phi_{J-1,k}(x)$ at scale $(J-1)$, but not orthogonal to the box functions $\Phi_{Jk}(x)$ at scale J.

To recover the lost detail, the 2^J orthogonal basis functions are chosen as $\{\Phi_{J-1,k}(x),\Psi_{J-1,k}(x)\}$ to obtain the expansion

$$n^{(J)}(x)=\sum_{k=0}^{2^{(J-1)}-1}\ [n_{J-1,k}\ \ \Phi_{J-1,k}(x)+\widetilde{n}_{J-1,k}\Psi_{J-1,k}(x)]. \tag{7}$$

Notice that unlike the box functions $\Phi_{Jk}(x)$, the difference functions $\Psi_{Jk}(x)$ from different scales J are orthogonal to one another and can be taken as the orthogonal basis functions for expansion. In practice, the procedure is as follows: At first, the orthogonal basis functions are the set $\{\Phi_{Jk}(x)\}$. Down to the scale $(J-1)$, the set $\{\Phi_{J-1,k}(x),\Psi_{J-1,k}(x)\}$ is taken. The information lost by the rougher resolution of the box functions $\Phi_{J-1,k}(x)$ is recovered by the difference functions $\Psi_{J-1,k}(x)$. Down to the next lower scale $(J-2)$, the set becomes $\{\Phi_{J-2,k}(x),\ \Psi_{J-2,k}(x),\Psi_{J-1,k}(x)\}$. Again, the information lost by the box functions $\Phi_{J-2,k}(x)$ is recovered by the difference functions $\Psi_{J-2,k}(x)$. Then, the set $\{\Phi_{J-3,k}(x),\Psi_{J-3,k}(x),\Psi_{J-2,k}(x),\Psi_{J-1,k}(x)\}$ is taken. Finally, one has the set $\{\Phi_{00}(x),\Psi_{00}(x),\Psi_{1k}(x),\Psi_{2k}(x),\ \ldots,\Psi_{J-1,k}(x)\}$. Notice that the number of the basis functions is always 2^J. The final expansion is given as

$$n^{(J)}(x)=n_{00}\Phi_{00}(x)+\sum_{j=0}^{J-1}\sum_{k=0}^{2^j-1}\ \widetilde{n}_{jk}\Psi_{jk}(x), \tag{8}$$

where the coefficients $\widetilde{n}_{jk}$ are called the wavelet amplitudes and the indices j,k are referred to as the scale index j and the position index k. As $\Phi_{00}(x)=1$, the coefficient n_{00} is merely the average of the distribution $n^{(J)}(x)$:

$$n_{00}=\int_0^1 dx\ n^{(J)}(x). \tag{9}$$

Compared to the regular expansion in the box functions in Eq. (1), which is implemented at a fixed scale J, the expansion in difference functions in Eq. (8) involves many scales. Going from one scale j to the next lower scale $(j-1)$, only the difference between the two resolutions is memorized in the wavelet amplitudes.

In general, the difference function $\Psi_{jk}(x)$ is called a wavelet and the box function $\Phi_{jk}(x)$ the corresponding scaling function, both of which can be constructed from two functions by a discrete dilation factor 2^j and a translation governed by the integer k,

$$\Psi_{jk}(x)=\Psi(2^jx-k), \tag{10}$$

$$\Phi_{jk}(x)=\Phi(2^jx-k), \tag{11}$$

where $\Psi(x)\equiv\Psi_{00}(x)$ and $\Phi(x)\equiv\Phi_{00}(x)$ are defined at the roughest scale. Furthermore, these two functions can be related through the fundamental dilation equations as

$$\Psi(x)=\sum_m\ (-1)^m c_{1-m}\Phi(2x-m), \tag{12}$$

$$\Phi(x)=\sum_m\ c_m\Phi(2x-m), \tag{13}$$

where the coefficients c_m specify the functions $\Phi(x)$ and $\Psi(x)$ [1]. In practice, a finite set of the coefficients $\{c_m\}$ is given. The function $\Phi(x)$ is then solved from Eq. (13) by self-consistent iterations. The function $\Psi(x)$ is obtained with Eq. (12). Then, the entire family of wavelets and scaling functions can be found with Eqs. (10) and (11). Obviously, the values of the coefficients c_m are not arbitrarily chosen. Various constraints must be satisfied [1]. For example, the integration on both sides of Eq. (13) implies

$$\sum_m\ c_m=2. \tag{14}$$

The special case of box functions and difference functions in Eqs. (2) and (4) represents the simplest example known as Haar wavelet; moreover, there are only two nonvanishing coefficients: $c_0=c_1=1$. Since the discrete counting problem, i.e., the multiplicity fluctuations, is the main concern, the discontinuity of Haar wavelets is not a serious drawback, as it appears to be in some other fields.

III. MULTIPLICITY FLUCTUATIONS

In this section wavelet analysis is used to study and compare the multiplicity fluctuations in three different models: the FRITIOF, random cascade, and Ising models. The procedure is as follows: a number of particle configurations is generated via the Monte Carlo method with the mechanism specified by each model. For each configuration, the particle distribution is expanded and the amplitudes n_{Jk} and $\widetilde{n}_{jk}$ are obtained with Eqs. (1) and (8), respectively. Then the bin correlation $\langle n_{Jk}\cdot n_{Jk'}\rangle$ and the wavelet correlation $\langle\widetilde{n}_{jk}\cdot\widetilde{n}_{j'k'}\rangle$ are calculated, where angular brackets denote the ensemble average. Notice that at the finest resolution scale J, the indices $k,k'=0,1,2,\ldots,(2^J-1)$ in the bin correlation and the indices $j,j'=0,1,2,\ldots,(J-1)$ and $k,k'=0,1,2,\ldots,(2^j-1)$ in the wavelet correlation.

The moment spectrum $\langle M_j\rangle$ and wavelet spectrum $\langle E_j\rangle$ are also calculated and defined as

$$M_j\equiv\frac{1}{2^J-2^{J-j}+1}\sum_{i=0}^{2^J-2^{J-j}}\left(\frac{1}{2^{J-j}}\sum_{k=0}^{2^{J-j}-1}\ n_{J,k+i}\right)^2, \tag{15}$$

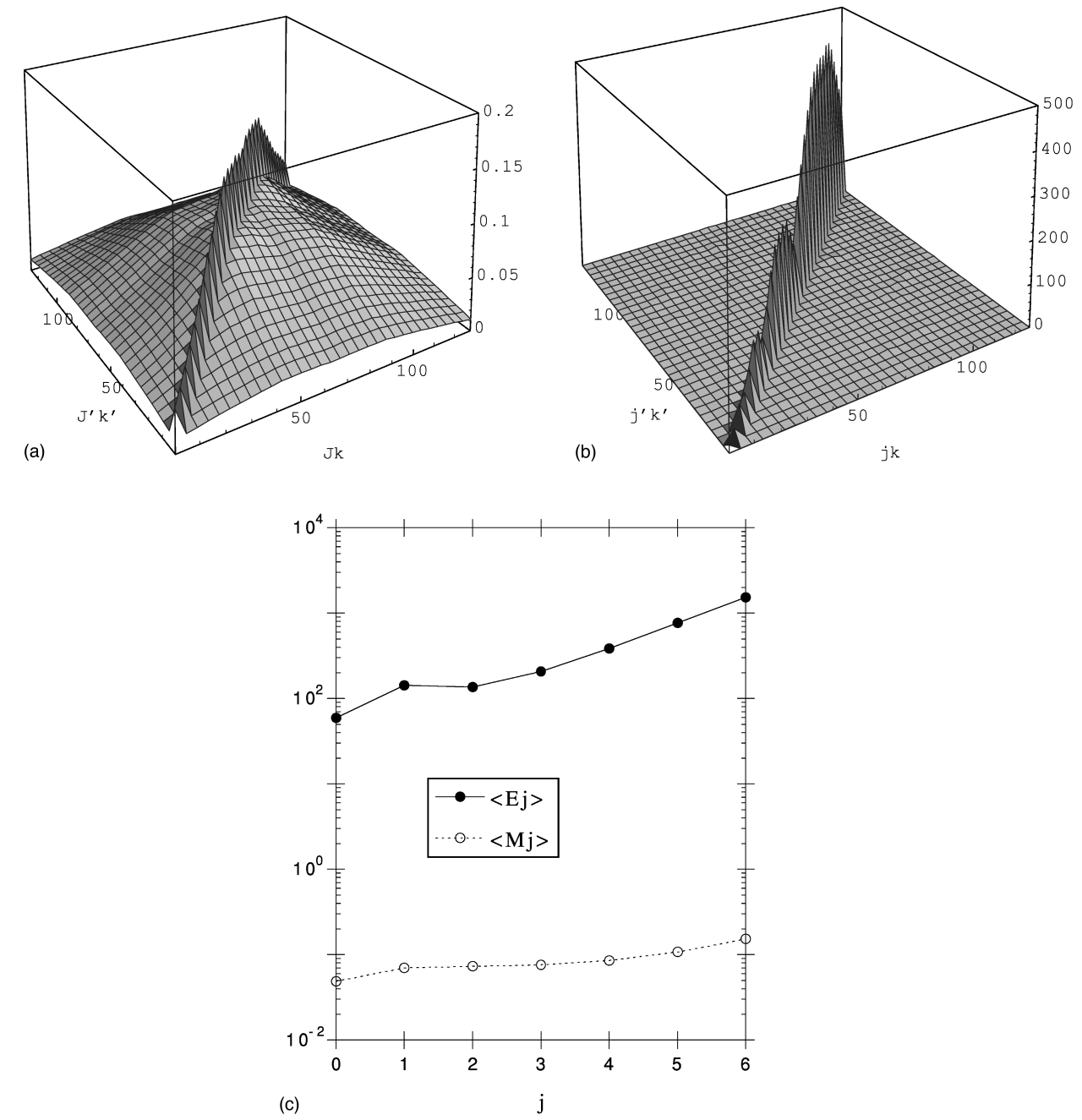

FIG. 1. Multiplicity fluctuations in the FRITIOF model at $\sqrt{s}=540$ GeV. (a) Bin correlation $\langle n_{Jk}\cdot n_{J'k'}\rangle$. The indices (Jk) are understood as k and range from 0 to 127. (b) Wavelet correlation $\langle \tilde{n}_{jk}\cdot \tilde{n}_{j'k'}\rangle$. The indices (jk) are understood as (2^j+k-1) and range from 0 to 126. (c) Moment spectrum $\langle M_j\rangle$ and wavelet spectrum $\langle E_j\rangle$. The index j ranges from 0 to 6.

$$E_j \equiv \frac{1}{2^j}\sum_{k=0}^{2^j-1}(\tilde{n}_{jk})^2, \tag{16}$$

where the index $j=0,1,2,\ldots,(J-1)$. Notice that the moment spectrum $\langle M_j\rangle$ can be identified with the conventional second-order moment at scale j. The entire interval of 2^J bins is divided into 2^j parts, i.e., the resolution is set to a coarse bin consisting of $2^{(J-j)}$ bins. The summation over k gives the particle number within one of the coarse bins; and the summation over i returns the average over different coarse bins. For the wavelet spectrum $\langle E_j\rangle$, the summation over k is simply the average over the amplitudes obtained at scale j. The wavelet spectrum E_j is also known as the power spectrum, which is then the power of fluctuations, with respect to the wavelet basis at scale j. Similar to the Fourier analysis, a Parseval theorem for wavelets can be established utilizing the complete and orthonormal properties of the wavelets:

$$\int_0^1 [n(x)]^2 dx = \sum_{j=0}^{J-1}\frac{1}{2^j}\sum_{k=0}^{2^j-1}(\tilde{n}_{jk})^2. \tag{17}$$

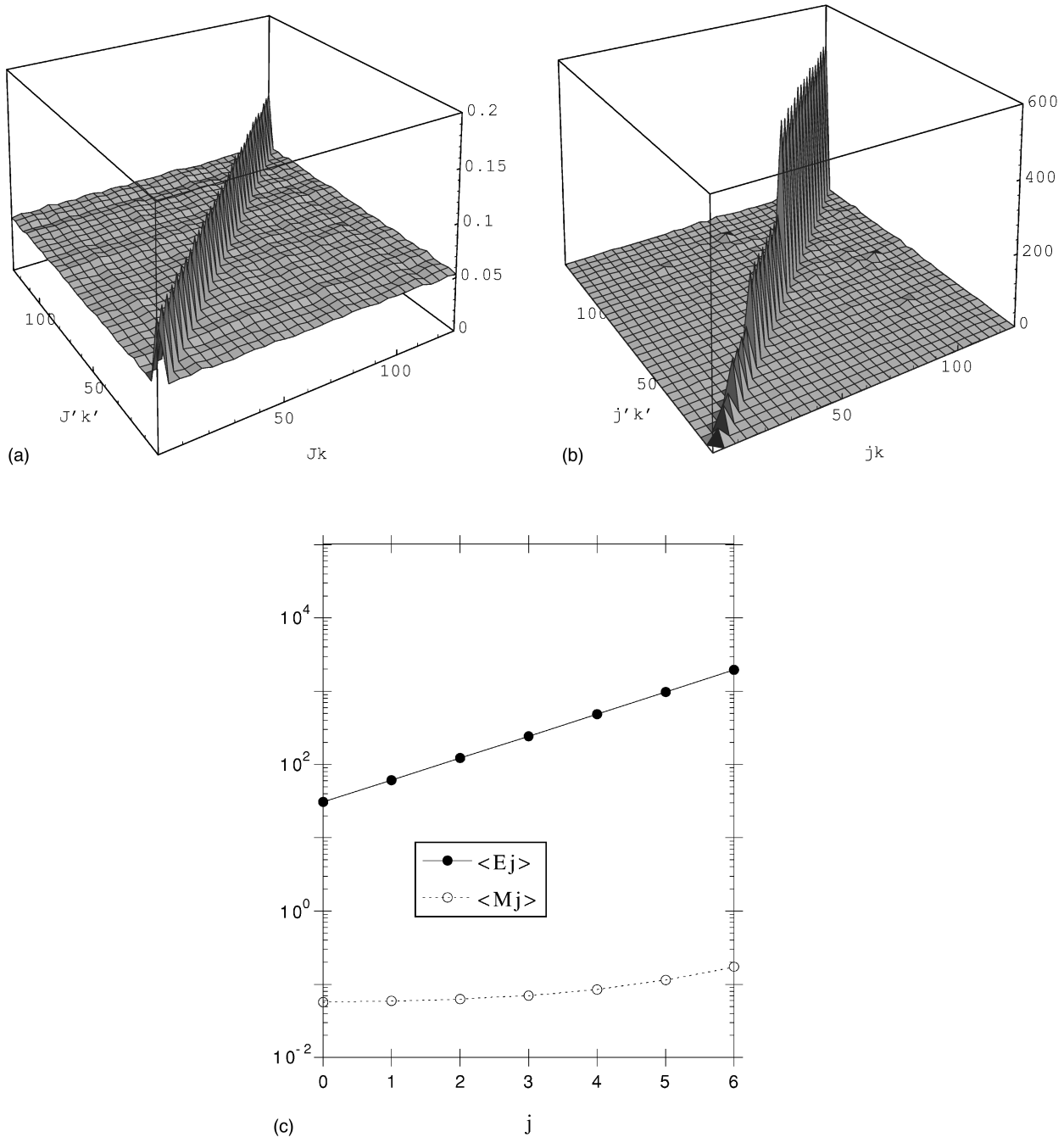

FIG. 2. Same as Fig. 1 for the p model with parameters $p=0.5$ and $n_0=30$.

A. FRITIOF model

The QCD-inspired FRITIOF model is a widely used Monte Carlo simulation in studies of the high-energy multiparticle production process [9]. The model is based on semiclassical considerations of string dynamics. The basic idea is that a hadron behaves like a relativistic string with a confined color field similar to the vortex line in a type II superconductor. The field of such a vortex line can be depicted as a chain of dipoles lined up along the vortex line. These dipole links behave exactly like partons. During the collisions many small transverse momenta are exchanged between the dipole-links and result in two longitudinally excited strings. Disturbance of the color field will initialize gluonic radiation according to the QCD, which can then be naturally incorporated in this picture by the color dipole approximation. The final state particles are obtained by fragmenting the string, precisely like the usual strings in an e^+e^- annihilation described by the Lund model.

In this study 50 000 minimum-biased events of $\overline{p}p$ collisions at CERN Super Proton Synchrotron energy $\sqrt{s}=$ 540 GeV are generated with the default parameters. The final charged pions are recorded within the one-dimensional interval $\eta\in[-5,5]$, where η is the pseudorapidity defined as

$$\eta=\frac{1}{2}\ln\left(\frac{|\vec{P}|+P_{\parallel}}{|\vec{P}|-P_{\parallel}}\right)=\operatorname{arccosh}\left(\frac{1}{\sin\theta}\right), \tag{18}$$

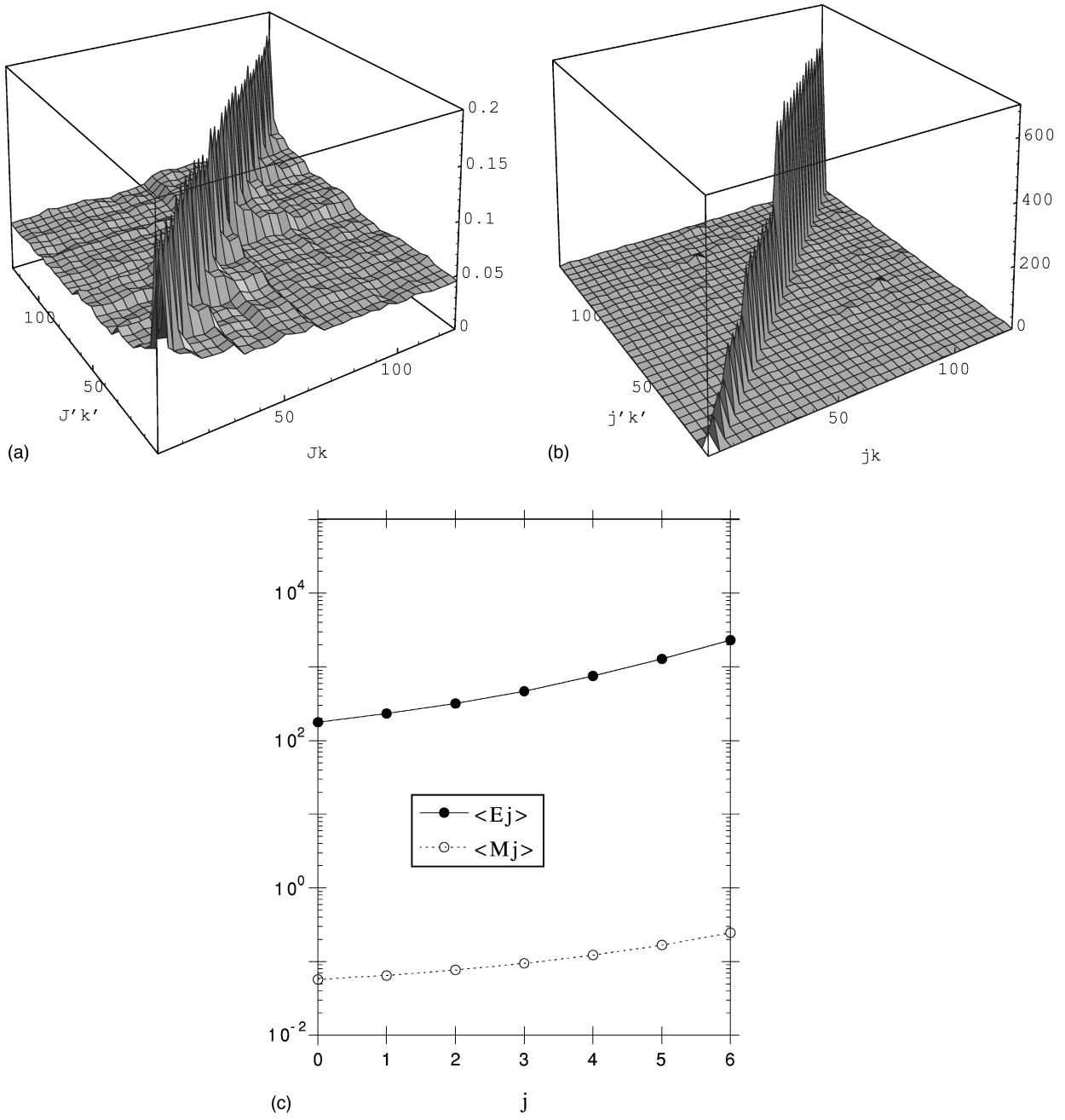

FIG. 3. Same as Fig. 1 for the p model with parameters $p=0.3$ and $n_0=30$.

where θ is the angle between the particle momentum $\vec{P}$ and the beam axis. To implement the wavelet analysis, the pseudorapidity interval $[-5,5]$ is divided into 128 bins, i.e., the resolution scale $J=7$. The resulting bin correlation $\langle n_{Jk}\cdot n_{J'k'}\rangle$ and wavelet correlation $\langle \tilde{n}_{jk}\cdot \tilde{n}_{j'k'}\rangle$ are shown in Figs. 1(a) and 1(b), respectively. As the figures show, the bin correlation $\langle n_{Jk}\cdot n_{J'k'}\rangle$ reveals large correlations in both diagonal and off-diagonal portions; while the off-diagonal contributions are suppressed in the wavelet correlation $\langle \tilde{n}_{jk}\cdot \tilde{n}_{j'k'}\rangle$. The implication is clear that the observed fluctuations are hierarchical and self-similar in nature, and the wavelets provide a good representation for studying the fluctuations.

The moment spectrum $\langle M_j\rangle$ and the wavelet spectrum $\langle E_j\rangle$ are shown in Fig. 1(c). The values of the moment spectrum $\langle M_j\rangle$ increase with an increase in scales j, i.e., an increase in resolution. This feature has been interpreted as resulting from the underlying fractal structure and named intermittency [12]. As shown in the figure, the wavelet spectrum $\langle E_j\rangle$ conveys the same information as the moment spectrum $\langle M_j\rangle$ does. The power-like behavior observed in the wavelet spectrum, i.e., $\ln\langle E_j\rangle \propto j$, indicates that the fluctuations are present in many scales. Similar features have been observed in two high-multiplicity JACEE events in a recent study [6].

B. Random cascade model

The p model is a self-similar random cascade model which successfully describes the multifractal spectrum of en-

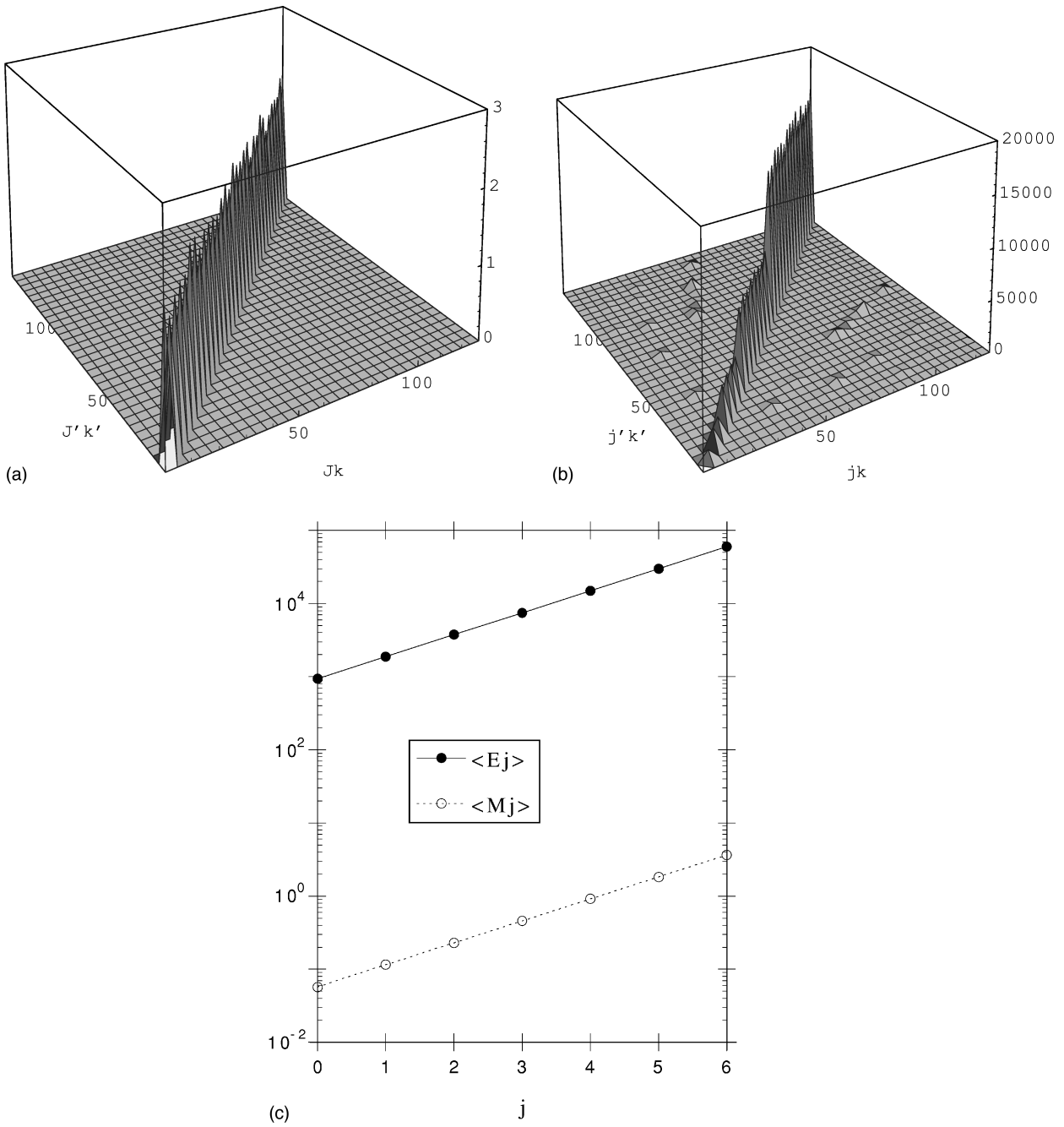

FIG. 4. Same as Fig. 1 for the p model with parameters $p=0$ and $n_0=30$.

ergy dissipation in a turbulent flow [10]. Consider the normalized energy E distributed within the interval $[0,1]$. This interval is then split into two equal parts with energies $E_1=pE$ and $E_2=(1-p)E$, where E_1 goes randomly to the left or right subinterval with equal probability and p is a free parameter. The left subinterval, assuming it accompanies the energy E_1, is then split again into two parts with corresponding energies $E_1'=pE_1$ and $E_2'=(1-p)E_1$, where, again, E_1' goes randomly to the new left or right subinterval. For the right subinterval one proceeds in the same manner. The whole procedure is repeated many times. After the J cascade steps, the energy distributed within the kth subinterval is denoted as ϵ_{Jk}, where the index $k=0,1,2,\ldots,(2^J-1)$. With the Poisson transformation introduced into intermittency studies [12], the continuous energy ϵ_{Jk} is replaced by a discrete multiplicity n_{Jk}. Each discrete random number n_{Jk} is tossed, independently from any other bin, according to a Poisson distribution

$$P(n_{Jk})=\frac{(n_0\epsilon_{Jk})^{n_{Jk}}}{n_{Jk}!}e^{-(n_0\epsilon_{Jk})}, \tag{19}$$

where n_0 is a free parameter denoting the average number of particles. In all, there are three parameters in the model: cascade steps J, splitting ratio p, and average multiplicity n_0. A symmetry is observed between the splitting ratio p and $(1-p)$. To compare with the fluctuations observed in the

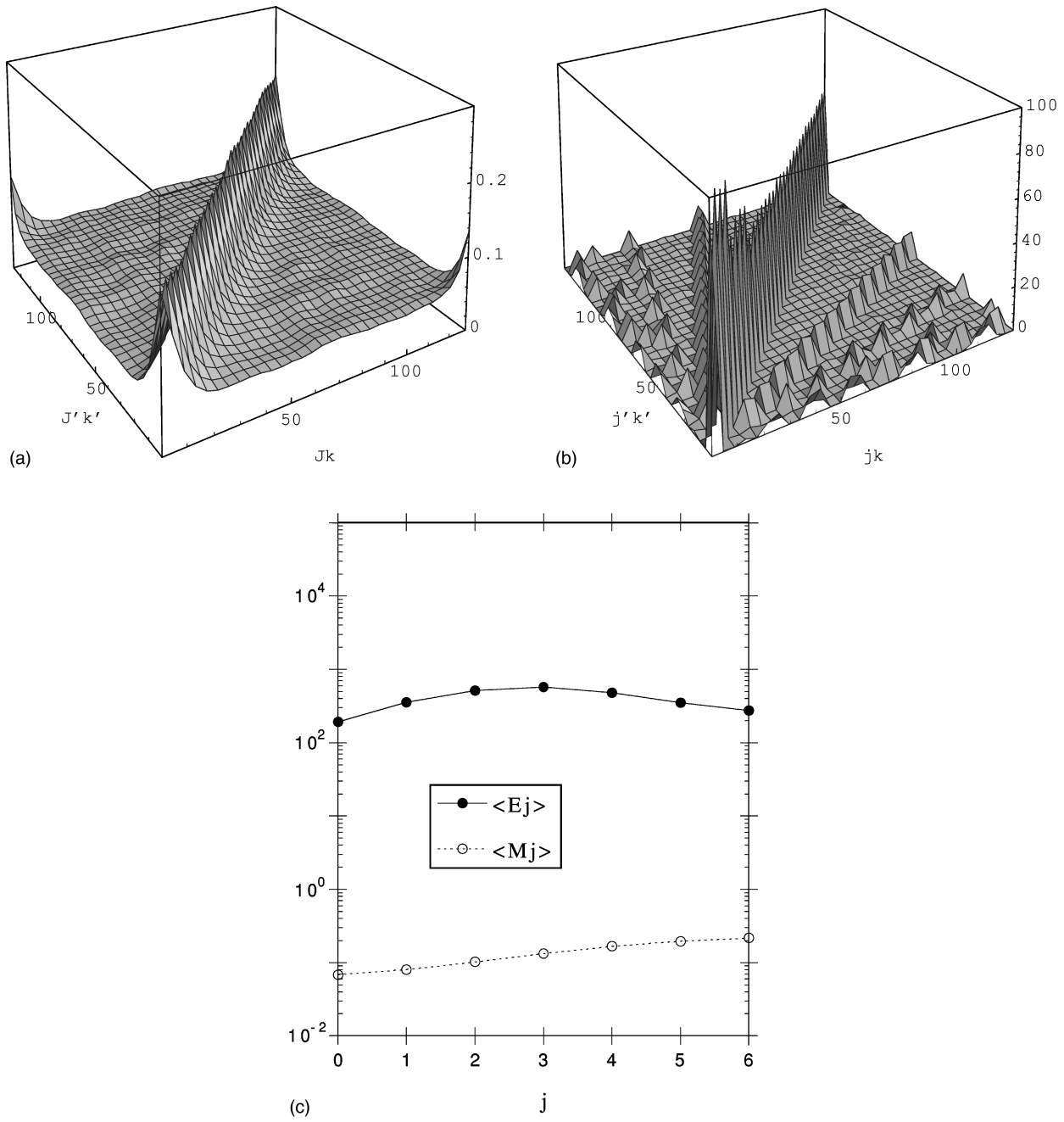

FIG. 5. Same as Fig. 1 for the Ising model on a lattice of 128 sites. The parameters are set at $\langle n\rangle = 30$ and $D = 15$.

FRITIOF model, the parameter n_0 is set at 30, which is the average multiplicity observed in the previous subsection.

Without the Poisson transformation, the Haar wavelets have been shown to provide adequate normal coordinates for the p model [5]. As the self-similarity in the p model is an intrinsic feature of the cascade splitting, introducing the Poisson transformation does not change the pattern qualitatively; the only exception is in the special case of $p = \frac{1}{2}$. Without the Poisson transformation there is no fluctuation, and the energy distributes uniformly when $p = \frac{1}{2}$, i.e., all ϵ_{Jk} are equal. After the Poisson transformation the fluctuations can be seen clearly in Fig. 2, where 10 000 Monte Carlo events have been generated with parameters $J = 7$, $p = 0.5$, and $n_0 = 30$. Again, the bin correlation $\langle n_{Jk} \cdot n_{J'k'}\rangle$ reveals correlations in both diagonal and off-diagonal portions; while the off-diagonal contributions are suppressed in the wavelet correlation $\langle \tilde{n}_{jk} \cdot \tilde{n}_{j'k'}\rangle$. These fluctuations can be interpreted as resulting from the Poisson noises; in the case of $p = 0.5$, the self-similar cascade is irrelevant.

As the value of parameter p deviates from 0.5, the fluctuations increase. In Fig. 3, the results are shown for $p = 0.3$, $J = 7$, and $n_0 = 30$. In the limiting case of $p = 0$, i.e., the largest fluctuations, the results are shown in Fig. 4.

For the bin correlation $\langle n_{Jk} \cdot n_{J'k'}\rangle$, the Poisson noises present a uniform off-diagonal contribution, as in Fig. 2(a). As p deviates from 0.5, the self-similar cascade introduces a correlation which declines along the off-diagonal direction and is uniformly enhanced along the diagonal direction, as in Fig. 3(a). In the limiting case of $p = 0$, the diagonal contributions are further enhanced and the off-diagonal contribu-

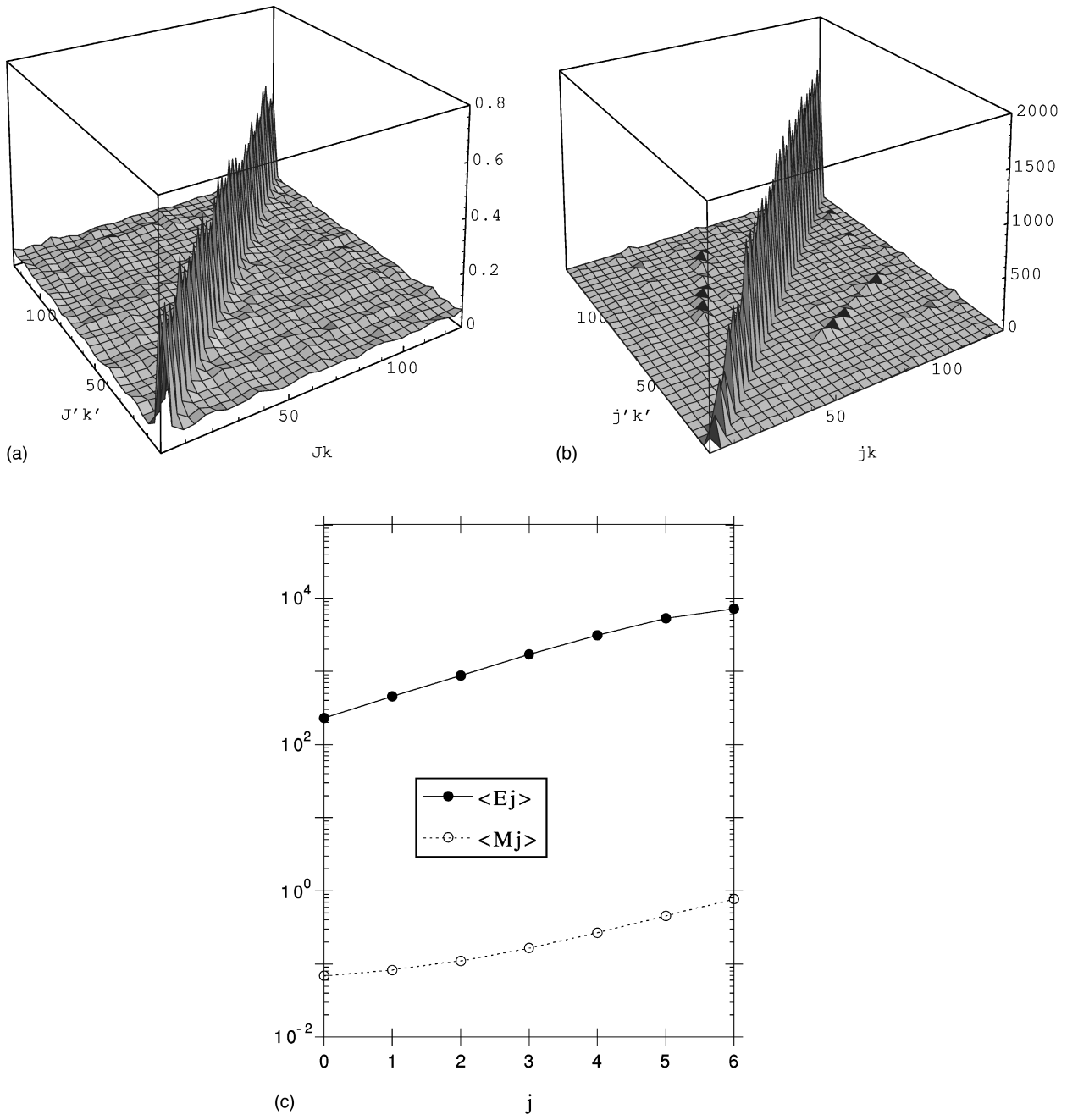

FIG. 6. Same as Fig. 1 for the Ising model on a lattice of 1280 sites. The parameters are set at $\langle n\rangle = 30$ and $D = 15$.

tions become negligible, as in Fig. 4(a). As for the moment spectrum $\langle M_j\rangle$, the dependence on the splitting ratio p increases with an increase in j. The values of $\langle M_0\rangle$ are independent of the values of p, while the values of $\langle M_6\rangle$ increase significantly as the values of p vary from 0.5 to 0.

As shown in Figs. 2(b), 3(b), and 4(b), the observed fluctuations in the wavelet correlation $\langle \tilde{n}_{jk} \cdot \tilde{n}_{j'k'}\rangle$ are similar to those of Poisson noises with enhanced amplitudes. The variation in the splitting ratio p can be seen clearly in the wavelet spectrum $\langle E_j\rangle$. As the values of p deviate from 0.5, the enhancement of $\langle E_j\rangle$ is first observed in the smaller values of j, i.e., the rougher resolution. As the values of p further decrease, the enhancement of $\langle E_j\rangle$ becomes dominated by the larger values of j, i.e., the finer resolution. In the limiting case of $p = 0$, a power law behavior is recovered, as in Fig. 4(c).

C. Ising model

The Ising model is a classical spin model with the Hamiltonian [11]

$$H = -\epsilon \sum_{\langle i,j\rangle} S_i \cdot S_j + b \sum_i S_i , \tag{20}$$

where $\langle i,j\rangle$ denotes the summation over nearest-neighbor sites and the spins S_i assume values of ± 1. The ferromagnetic strength ϵ and the external magnetic field b are two free parameters of the model. With lattice-gas interpretation, $n_i \equiv 1/2(S_i + 1)$, the Ising model can be used to study the multiplicity fluctuations [15]. For comparison with the fluctuations presented in other models, the two parameters ϵ and

b are adjusted to reproduce the average multiplicity $\langle n\rangle = 30$ and dispersion $D \equiv \sqrt{\langle n^2\rangle - \langle n\rangle^2} = 15$, which are the values observed in the FRITIOF model in Sec. III A.

To perform an analysis with a resolution scale $J=7$, the lattice must contain at least 128 sites. The results on a lattice of 128 sites are shown in Fig. 5, where 10 000 Monte Carlo events are recorded. The bin correlation $\langle n_{Jk}\cdot n_{J'k'}\rangle$ presents a feature similar to the Poisson noise in Fig. 2(a). Uniform off-diagonal contributions are superimposed with a uniform peak of diagonal contributions. It is noticed that the peak along the diagonal direction is not so sharp as in the Poisson noise. A rapid decline along the off-diagonal direction is observed. The increase on the off-diagonal corner is due to periodic boundary conditions. The features revealed by wavelet correlation $\langle \tilde{n}_{jk}\cdot \tilde{n}_{j'k'}\rangle$ are quite different from those of the Poisson noise. Again, the off-diagonal contributions are effectively suppressed. The remaining off-diagonal contributions rise in bands, which implies that the correlations between different scales can be interpreted as the result of self-similarity like the cascading in the p model. The downward curve observed in the wavelet spectrum $\langle E_j\rangle$ is obviously the effect of the finite lattice.

On a larger lattice the fluctuations are enhanced and become similar to those observed in the p model. The results on the lattice of 1280 sites are shown in Fig. 6. To keep the constraints $\langle n\rangle = 30$ and $D=15$ in the simulations, the values of ϵ and b must increase with the number of lattice sites; while in the conventional thermodynamic limit, the values of ϵ and b are kept fixed. As shown in the figures, uniform off-diagonal contributions in bin correlation $\langle n_{Jk}\cdot n_{J'k'}\rangle$ can still be observed. The remaining off-diagonal contributions in wavelet correlation $\langle \tilde{n}_{jk}\cdot \tilde{n}_{j'k'}\rangle$ still rise in bands. The downward curve in the wavelet spectrum $\langle E_j\rangle$ disappears.

IV. CONCLUSIONS

In this study wavelet analysis has been used to study the multiplicity fluctuations in three different models. Generally, the large off-diagonal bin correlations are effectively suppressed by the wavelets. The correlations from different scales are nearly decoupled, i.e., the wavelet-transformed distribution takes a quasidiagonal form. Moreover, the diagonal contributions from different scales exhibit a scaling law, i.e., a powerlike behavior is observed. Such features arise naturally in the random cascade model, where self-similarity is an intrinsic feature. It has been observed that the same features can also result from the nearest-neighbor interactions of the Ising model.

The multiresolution feature of wavelet analysis is essential for identification of the structure of interest, since the wavelet transformation suppresses redundancy in the correlation information, behaving like a mathematical microscope which can zoom in or out to various scales at each location. It was expected that data arising from hierarchically organized random processes exhibit a uniquely simple correlation structure once they are represented on an appropriate wavelet basis.

Because of the completeness and orthogonality of the wavelet basis, there is no information loss. In the expansions in Eqs. (1) and (8), the wavelet amplitudes $\{\tilde{n}_{jk}\}$ carry exactly the same information as the bin amplitudes $\{n_{Jk}\}$ do. Specifically, the transformation between these two sets can be easily obtained as

$$\tilde{n}_{J-1,k} = \tfrac{1}{2}(n_{J,2k} - n_{J,2k+1}), \tag{21}$$

$$\tilde{n}_{J-2,k} = \tfrac{1}{4}(n_{J,4k} + n_{J,4k+1} - n_{J,4k+2} - n_{J,4k+3}), \tag{22}$$

$$\vdots$$

In general, one has

$$\tilde{n}_{jk} = \frac{1}{2^{J-j}} \sum_{l=0}^{1} \sum_{\{k'\}} (-1)^l n_{Jk'}, \tag{23}$$

where the index $k' \equiv (2^{J-j}k + 2^{J-j-1}l + i)$ and $\{k'\}$ denotes the summation over index i from 0 to $(2^{J-j-1}-1)$.

In conclusion, wavelet analysis is expected to serve as a useful tool for studying the self-similar aspects of QCD parton cascades occurring in e^+e^- and hadron-hadron collisions.

[1] I. Daubechies, *Ten Lectures on Wavelets* (SIAM, Philadelphia, 1992).

[2] C. Chui, *An Introduction to Wavelets* (Academic, Philadelphia, 1992).

[3] Y. Meyer, *Wavelets and Operators* (Cambridge University Press, Cambridge, England, 1993).

[4] G. Kaiser, *A Friendly Guide to Wavelets* (Birkhäuser, Boston, 1994).

[5] M. Greiner, P. Lipa, and P. Carruthers, Phys. Rev. E **51**, 1948 (1995); M. Greiner, J. Giesemann, P. Lipa, and P. Carruthers, Z. Phys. C **69**, 305 (1996).

[6] N. Suzuki, M. Biyajima, and A. Ohsawa, Prog. Theor. Phys. **94**, 91 (1995); Report No. hep-ph/9702348.

[7] Z. Huang, I. Sarcevic, R. Thews, and X. N. Wang, Phys. Rev. D **54**, 750 (1996); Report No. hep-ph/9607224.

[8] N. M. Astafyeva, I. M. Dremin, and K. A. Kotelnikov, Report No. hep-ex/9705003.

[9] B. Andersson, G. Gustafson, and B. Nilsson-Almqvist, Nucl. Phys. **B281**, 289 (1987); B. Andersson, G. Gustafson, and H. Pi, Z. Phys. C **57**, 485 (1993); B. Nilsson-Almqvist and E. Stenlund, Comput. Phys. Commun. **43**, 387 (1987); H. Pi, *ibid.* **71**, 173 (1992).

[10] C. Meneveau and K. R. Sreenivasan, Phys. Rev. Lett. **59**, 1424 (1987).

[11] E. Ising, Z. Phys. **31**, 253 (1925).

[12] A. Biakas and R. Peschanski, Nucl. Phys. **B273**, 703 (1986); **B308**, 857 (1988).

[13] P. Lipa and B. Buschbeck, Phys. Lett. B **223**, 465 (1989).

[14] L. L. Chau and D. W. Huang, Phys. Lett. B **283**, 1 (1992); Phys. Rev. Lett. **70**, 3380 (1993).

[15] For example, see Kerson Huang, *Statistical Mechanics* (Wiley, New York, 1987), Chap. 14.